Fluid Chemical and Isotopic Signatures Insighting the Hydrothermal Control of the Wahongshan-Wenquan Fracture Zone (WWFZ), NE Tibetan Plateau

Tingxin Li , Rui Lu , Wenping Xie , Jinshou Zhu , Lingxia Liu , Wenjing Lin *

Posted Date: 11 April 2024

doi: 10.20944/preprints202404.0757.v1

Keywords: Hydrogeochemistry; geothermal gas isotopes; geothermal systems; NE Tibetan Plateau

 doi:10.20944/preprints202404.0757.v1

Article

Fluid Chemical and Isotopic Signatures Insighting the Hydrothermal Control of the Wahongshan-Wenquan Fracture Zone (WWFZ), NE Tibetan Plateau

Tingxin Li [1,2], Rui Lu [3,4], Wenping Xie [3,4], Jinshou Zhu [3,4], Lingxia Liu [1,2], Wenjing Lin [1,2,*]

[1] Institute of Hydrogeology and Environmental Geology, Chinese Academy of Geological Sciences, Shijiazhuang, China
[2] Technology Innovation Center for Geothermal & Hot Dry Rock Exploration and Development, Ministry of Natural Resources, Shijiazhuang, China
[3] Qinghai Geological Survey Bureau, Xining, China
[4] Technology Innovation Center for Exploration and Exploitation of Strategic Mineral Resources in Plateau Desert Region, Ministry of Natural Resources, Xining, China
* Correspondence: linwenjing@mail.cgs.gov.cn

Abstract: Compared to the southern Tibetan Plateau, the northern part has been regarded as relatively lacking geothermal resources. However, there is no lack of natural hot springs exposed in beads along large-scale fracture systems, and research on them is currently limited to individual hot springs or geothermal systems. This paper focuses on the Wahongshan-Wenquan Fracture Zone (WWFZ), analyzes the formation of five hydrothermal activity zones along the fracture zone in terms of differences in the hydrochemical and isotopic composition of the hot water, and then explores the hydrothermal control of hot springs in the zone by the fracture. The results show that the main Fractures of WWFZ is the regional heat-control structures, and the fracture system formed by a small number of near-north-south and near-east-west fractures transversal to it provides a favorable channel for deep hydrothermal convective circulation. Ice and snow melt water from the Ngola Shan Mountains, with an average elevation of more than 4,500 meters above sea level, infiltrates along the fractures and is heated by deep circulation to form deep geothermal reservoirs. There is no detectable contribution of mantle source heat to the hot spring gases, and the heat source is mainly natural heat conduction warming, but the "Low-Velocity body (LVB)" in the middle and lower crust of the area may be the primary heat source of the high geothermal background in the area. The hydrochemical components of the hot springs in the area show a certain regularity, and the main ionic components, TDS and water temperature, tend to increase away from the main rupture, reflecting the controlling effect of the WWF on the hydrothermal transport in the area. In the future, the geothermal work in this area should focus on the hydrothermal control properties of different levels, the nature of fractures in the area, and the thermal contribution of LVB in the middle and lower crust.

Keywords: hydrogeochemistry; geothermal gas isotopes; geothermal systems; Wahongshan-Wenquan Fracture Zone (WWFZ)

1. Introduction

The Tibetan Plateau has the most vigorous geothermal activity in China, with the highest geothermal reserves in China and various surface geothermal manifestations throughout the region [1,2]. However, it is traditionally believed that the geothermal resources of the Tibetan Plateau are mainly concentrated in tectonically unstable areas such as southern Tibet, western Yunnan, and western Sichuan, while its northern and northeastern parts are in relatively stable blocks with average geothermal potential. Relevant studies have also focused on the north-south Himalayan rift zone [3–5], the Yunnan-Tibet geothermal zone [6,7], and several fault zones where hot springs in western Sichuan are relatively concentrated [8–14]. Only with the exploration of high-temperature Hot Dry Rock resources in Gonghe Basin on the northeastern margin of the Tibetan Plateau in recent years

 doi:10.20944/preprints202404.0757.v1

[15], has the region gained widespread attention and a large number of studies have been carried out to address the mechanism of the heat source and the potential for development [16–22].

The Wahongshan-Wenquan Fracture Zone (WWFZ) is located in the southwest of Gonghe Basin, which belongs to the southwest boundary fault of Gonghe Basin, controlling the contact between the basin and the East Kunlun Magma Belt (Figure 1). Several hot springs are exposed along the fracture zone in the NW-SE direction, indicating that the fracture controls the distribution of hot springs in the area to a certain extent. Therefore, the study on the genesis of hot springs in the area is of great significance for the in-depth understanding of the heat-control mechanism of the WWFZ and even for the in-depth analysis of the Gonghe Basin's high-temperature thermal background. Previous authors have conducted relevant analyses for some hot springs in the area. Zhang et al. (2016) carried out the principal component analysis of the chemical composition of some hot spring water in the area [23]. They proposed the geochemical genesis of the main components in the hot water and the related hydrogeochemical processes. Ma et al. (2020) carried out a fluid geochemical and water-rock interaction study of the hot water in the southeastern section of the WWFZ [24]. They proposed that the dissolution and recrystallization of aluminosilicate minerals in hot water is the most crucial hydrogeochemical process controlling the content of cations in hot water. In contrast, the under-seepage of recharging water and the dissolution and filtration of saline minerals in the geothermal runoff and upwelling process are the primary sources of anions in the water. Wang et al. (2023a) studied the geochemical analysis and genesis mechanism of the hot springs on the southwest side of the fracture [25]. They proposed that the hot springs belong to a deep-circulating convective geothermal system controlled by the fracture, with a geothermal reservoir temperature as high as 245-261 ℃ and a deep circulation depth of 7,700-8,200 m. The previous studies focused on the individual hot springs in the area. They lacked comparative analyses on the elements of different geothermal systems in the area and the mechanisms of their genesis.

The geotectonic context in which a geothermal system is located is the result of the long-term evolution of the Earth, which governs the temperature, fluid composition, and reservoir characteristics of the geothermal system and determines its specific type (convective or conductive) [26]. Geothermal fields around the world are invariably tectonically controlled. Fractures are the most prevalent heat-controlling tectonics. Under favorable geological and tectonic conditions, meteoric water seeps down along the fracture is warmed by deep circulation, and then gathers and surges upward to be exposed on the surface along different high-angle fracture zones or steeply inclined permeable strata. Thus, bead-like localized thermal anomaly zones can be formed near the fracture zones. In this paper, geothermal fluid and gas geochemical samples from different geothermal anomalies in the WWFZ were systematically collected and combined with the regional geologic and tectonic conditions, comparative analyses of fluid geochemistry, geothermal reservoir characteristics, and heat source mechanism of different geothermal systems were systematically carried out to explore the role of the WWFZ fracture zone in controlling the geothermal systems in the area and to provide reference for further geothermal exploration in this area in the future.

 doi:10.20944/preprints202404.0757.v1

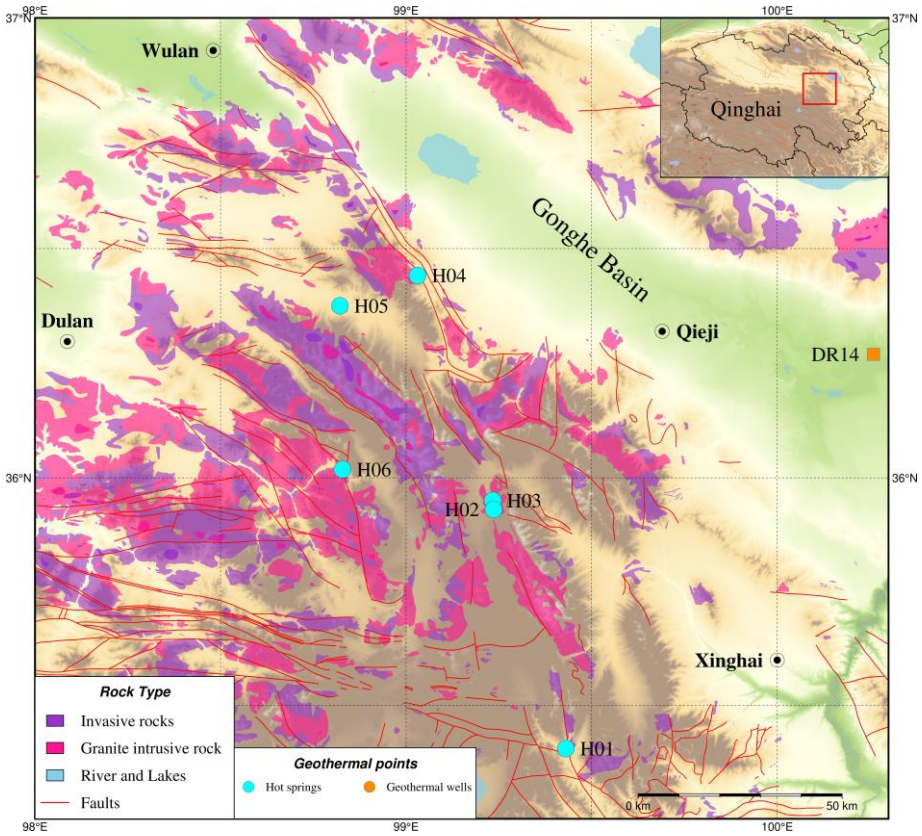

Figure 1. Geologic sketch of the Wahongshan-Wenquan Fractures Zone (WWFZ) and distribution of hot springs.

2. Materials and Methods

2.1. Study Area

The WWFZ fracture zone starts from Agushar in the south, passes through the Harihad Mountains, and ends in Changshui in the south, with a length of about 275 km, and in the study area, it is about 200 km long. The main tectonic trace of the fracture zone is NW-NNW oriented, which consists of several high-angle reverse faults trending in the north-northwestern direction, and it is an extrusive reverse strike-cum-rightward strike-slip fracture [27]. A few small-scale near-north-south and near-east-west oriented fractures cut the geologic body into diamond-shaped fracture blocks. Along the fracture zone, there is extensive development of banded bedrock and intermittently distributed ultramafic rocks, and locally, moderate-acid intrusive rocks can be seen. The fracture has a considerable depth of influence and is a crustal fracture. The fracture was formed at the end of the Early Paleozoic Era, and its activity increased from the Hualixi Period to the middle Indo-Chinese Period. In the late Indo-Chinese-Himalayan period, the region entered the stage of intra-land orogeny, and the WWFZ fracture and a series of basically synchronized fractures formed the north-northwestern Erasan slip tectonic zone with right-lateral slip, which controlled the intrusion of the middle-acidic magmatism in the Indo-Chinese period and the distribution of the regional Late Triassic volcano-sedimentary basins. The distribution of small seismic groups in an active tectonic structure characterizes the fracture zone.

Along the WWFZ, there are hot springs distributed in Wenquan Township, Xinghai County (H01, 31-64°C), North and South Hot Springs, Sangchigou, Xinghai County (H02 and H03, 65-78°C), Bayinggeri Hot Springs, Dulan County (H04, 35-46°C), Angutan Hot Springs, Dulan County (H05, 67°C), and Reshuigou Hot Springs, Dulan County (H06, 87°C), and most of these hot springs are located at the intersection of different fractures with near-north-south and near-east-west oriented fractures within the WWFZ (Figure 1). Most of these hot springs are in a primitive and undeveloped

 doi:10.20944/preprints202404.0757.v1

state, except for the hot springs(H01) in Wenquan Township, Xinghai County, which are currently under construction with related tourism and sanatorium facilities for tourists to bathe.

2.2. Sample Collection and Testing

The distribution of sampling sites is shown in Figure 1. The water chemistry and gas samples of hot water in the study area were collected by the project team from May to July 2022. A total of 6 sets of hot water samples and five sets of gas samples were collected from the area, and the testing items included complete analysis, trace elements, stable isotopes, conventional gas fractions, noble gas fractions, and isotopes. The water samples were first filtered through a 0.45 μm microporous filter membrane, then stored in polyethylene bottles, rinsed twice with deionized water, and dried. Hot water chemical composition and stable isotope analyses were conducted at the Institute of Hydrogeology and Environmental Geology, Chinese Academy of Geological Sciences. The FP640 flame photometer and PHS-25 digital acidimeter were utilized for chemical composition testing. The isotope testing instrument was a Model L2130i Water Isotope Analyzer, and measurements were expressed as thousandths of a percent relative to the VSMOW standard. Tritium was tested with a Quantulus Model 1220 Ultra Low Background Liquid Scintillation Spectrometer with an accuracy of ≤0.6 TU (1 TU is equivalent to 0.119 19 ± 0.00021 Bq-kg-1). The drainage method was used to collect hot spring gas samples. It was analyzed and tested at the Oil and Gas Resources Research Center of the Northwest Institute of Ecology and Environmental Resources, Chinese Academy of Sciences (NWIER, CAS). He, Ne, and Ar gas concentrations and isotopes were analyzed using a Noblesse rare gas isotope mass spectrometer. Helium isotopes were tested with an error of ±10% for R-values above 1×10^{-7} and ±15% for R-values between 1×10^{-8} and 1×10^{-7}. The water chemistry and gas isotope composition of the different hot springs are shown in Tables 1 and 2.

Table 1. Chemical composition and stable isotope of hot springs in WWFZ.

ID	H/m	pH	T/℃	Chemical composition /(mg/L)									stable isotopes/‰		Recharge Elevation
				K^+	Na^+	Ca^{2+}	Mg^{2+}	Cl^-	SO_4^{2-}	HCO_3^-	TDS	SiO_2	δ^2H	$\delta^{18}O$	/m
H01	3945	7.91	64.0	21.9	267.0	41.8	5.3	169.0	329.0	140.0	1054	77.7	-90	-11.6	5155
H02	4282	8.29	78.0	13.7	303.0	24.3	3.9	296.0	186.0	116.0	1052	76.6	-92	-11.7	5525
H03	4282	8.29	60	11.66	301.9	25.42	0.51	232.5	301.7	110.4	1065	127.27	/	/	/
H04	3794	8.82	46.0	2.6	150.0	16.3	2.2	120.0	156.0	29.7	552	43.2	/	/	/
H05	3790	8.08	67.0	23.8	482.0	78.5	1.7	610.0	282.0	56.5	1704	108.5	-88	-12.2	5200
H06	4001	7.52	87.0	125.0	861.0	77.7	8.0	1461.0	36.3	134.0	2866	113.9	-85	-11.5	5178

Table 2. Gas composition and its isotopes of hot springs in WWFZ.

ID	gas componentsφB (%)							gas isotope		
	He	N_2	O_2	Ar	CO_2	CH_4	N_2/Ar	$^3He/^4He$	$^4He/^{20}Ne$	R/Ra
H01	0.1753	83.63	13.87	1.16	1.15	0.01	72.1	4.80E-08	101.03	0.03
H02	0.0142	79.29	18.53	0.96	1.2	-	82.6	1.00E-07	3.987	--
H04	0.0052	82.64	15.91	1.2	0.25	-	68.9	6.20E-08	7.22	--
H05	0.0375	73.67	17.3	1.13	7.83	0.04	65.2	3.90E-08	45.542	0.02
H06	0.0118	81.42	17.37	0.98	0.19	0.02	83.1	1.80E-08	11.921	--

 doi:10.20944/preprints202404.0757.v1

3. Results

3.1. Chemical Characterization of Hot Springs Water

The Schoeller diagrams of the chemical components of different hot springs in the study area are shown in Figure 2. Due to various geochemical processes occurring along the circulation path of the groundwater, the hot springs from different distances from the primary fracture of the WWFZ show different chemical compositional characteristics, but in general, the chemical composition of the hot spring water in the study area is relatively homogeneous. The cations are dominated by Na^+ ions, with concentrations ranging between 150.0-861.0mg/L. The Na^+ ion content of the hot springs near the primary fracture is around 300mg/L, and the lowest value occurs at H04, 46°C, where the spring water temperature is also the lowest. Away from the primary fracture, the Na^+ ion content increased significantly, with the highest value occurring at H06 and the highest spring temperature (87°C). Cl^- and SO_4^{2-} ions dominate the anions, with the ranges of 120.0-1461.0 and 36.3-329.0 mg/L, respectively. The trend of Cl^- was the same as that of Na^+ ions, and away from the primary fracture, the content of Cl^- ions in the hot springs was elevated, with the highest value occurring at H06. There is no obvious pattern in the change of SO_4^{2-} ions, which should be related to the strata through which the hot water of different hot springs flowed on the way up.

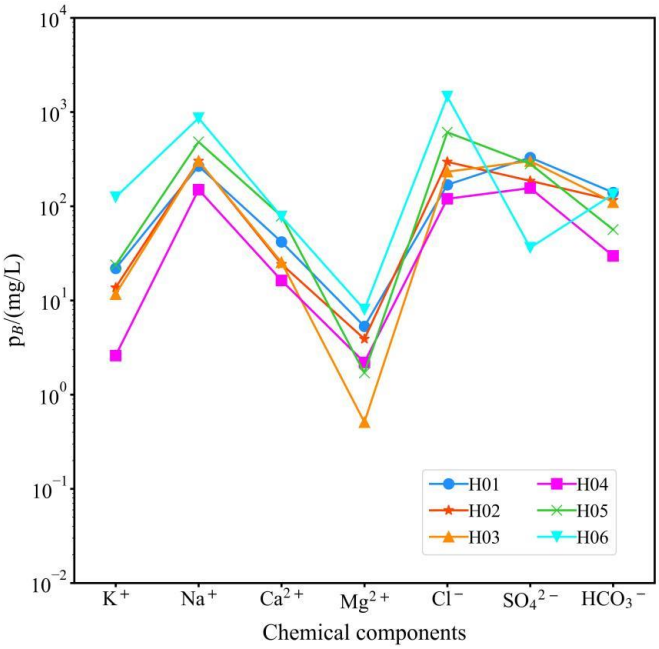

Figure 2. Schoeller diagram of chemical components of hot spring water in WWFZ.

In terms of hydrochemical types, the hot spring waters in the study area can be roughly categorized into the following two types: hot springs located near the primary fracture of the WWFZ are Cl-SO_4-Na or SO_4-Cl-Na type waters, including H01, H02, H03, and H04; those far away from the primary fracture show Cl-Na type waters, including H05 and H06. In general, however, the water chemistry of the hot springs in the WWFZ is mostly the same. All hot springs are clustered in the rightmost part of the diamond on the Piper diagram (Figure 3). However, the difference lies in the size of the TDS of the different hot springs, which ranges from 552 to 2866 mg/L, with the smallest value being H04, and the most considerable value occurring at H06, which is far away from the primary fracture.

 doi:10.20944/preprints202404.0757.v1

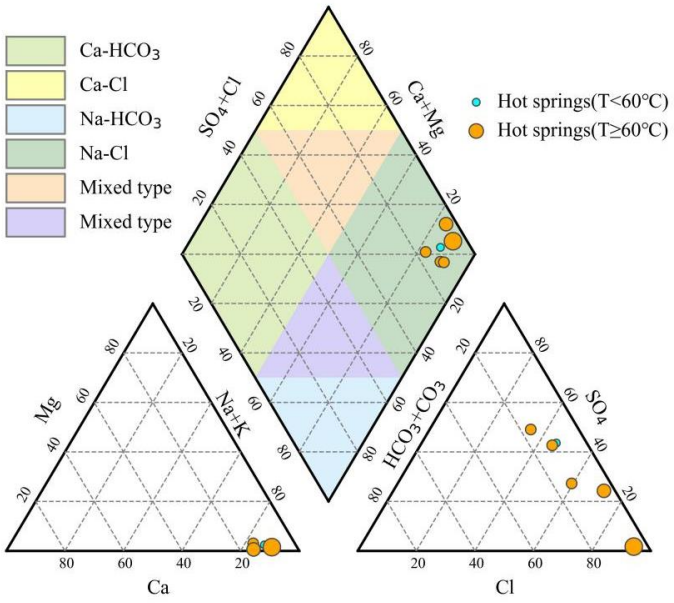

Figure 3. Piper diagram of hot spring water in WWFZ. The diameters of the different points in the diagram reflect the relative TDS content of the different hot springs.

Gibbs diagram is used to study the controlling factors for the formation of major ions in groundwater by using the relationship between Na^+, Ca^{2+}, Cl^-, HCO_3^- and TDS in water, which includes three types: evaporation-dominated, rock weathering-dominated, and precipitation-dominated. Plotting the Gibbs diagrams of different hot springs in the study area (Figure 4), it can be seen that the hot springs in the area generally have high temperatures, so their ions are evaporation-dominated, among which, H01 and H02, H03 are close to the rock weathering area, indicating that the hot springs have experienced some water-rock interactions. In contrast, H06 has a water temperature as high as 87 ℃, close to the local boiling point, and its chemical composition is dominated mainly by evaporation.

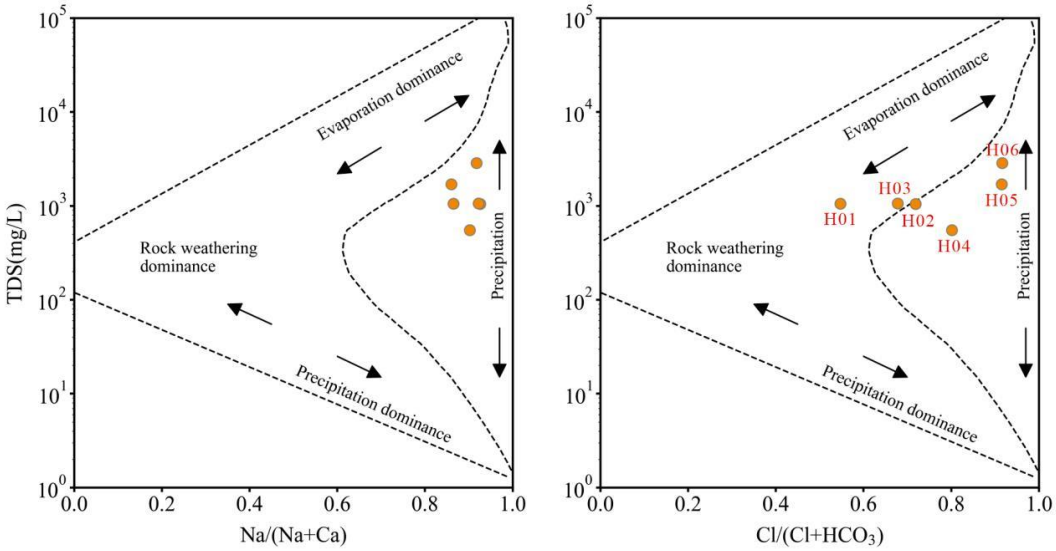

Figure 4. Gibbs diagram of hot spring water in Wahongshan-Wenquan Fractures zone.

The ratio between some ions in groundwater can help to analyze the various states and geological effects of groundwater, which can be used to analyze the hot water transport and hosting environment [28]. Different ionic characterization coefficients were calculated based on the water chemistry data of the hot springs in the study area, and the results are shown in Table 3. $\gamma Na^+/\gamma Cl^-$

 doi:10.20944/preprints202404.0757.v1

values characterize the groundwater metamorphism coefficients, which can respond to the confinement of the strata, the degree of metamorphism of the groundwater, and its activity. The smaller the value, the greater the degree of metamorphism, the better the environmental closure of the groundwater, and the greater the value, the greater the influence of the groundwater by infiltration water. It can be seen that far away from the main fracture of WWFZ, its $\gamma Na^+/\gamma Cl^-$ value gradually becomes smaller, reflecting that the environment tends to be closed, and the influence of surface and shallow groundwater recharge is gradually reduced. $\gamma Cl^-/\gamma Ca^{2+}$ value characterizes the hydrodynamic characteristics of groundwater, and the larger the value, the poorer the groundwater flow conditions are reflected and the slower the groundwater flow is. As can be seen in Table 3, except for H02 and H03, the flow conditions of hot water, in general, reflect that the flow conditions of hot water gradually become worse from the primary fracture to the two sides, and H02 and H03 are exposed in the open valley between the mountains. The flow conditions of hot water in them may have received the influence of the thicker quaternary cover on the surface. The salinization coefficient $\gamma Cl^-/(\gamma HCO_3^-)$ mainly reflects the concentration degree of stratum water, and the big value reflects the longer groundwater flow path and the slower water circulation. The $Cl^-/(\gamma HCO_3^-)$ values of the hot springs in the study area near the main fracture of the WWFZ are less than 7. In contrast, those of H05 and H06, which are far away from the main fracture, are greater than 18, which reflects that the turnover rate of the groundwater cycle is faster in the vicinity of the primary fracture and that the rate of the water cycle gradually slows down far away from the primary fracture.

Table 3. Ionic characterization coefficients of hot water in WWFZ.

ID	Ionic characterization coefficients		
	$\gamma Na^+/\gamma Cl^-$	$\gamma Cl^-/\gamma Ca^{2+}$	$\gamma Cl^-/\gamma HCO_3^-$
H01	2.44	9.11	2.07
H02	1.58	27.45	4.38
H03	2.00	20.61	3.62
H04	1.93	16.59	6.94
H05	1.22	17.51	18.55
H06	0.91	42.37	18.73

3.2. Hydrogen-Oxygen Stable Isotope Characterization of Hot Water

Deuterium and oxygen are stable isotopes in water, which can help identify the origin of groundwater, determine the hydraulic connection between groundwater, meteoric water, and surface water, and trace groundwater's recharge conditions and circulation pathways. The stable isotope δ^2H -$\delta^{18}O$ relationship of hot springs in the study area was plotted. The stable isotopes of geothermal wells, cold springs, salt lakes, rainwater, and snowwater in the Gonghe Basin adjacent to the WWFZ were collected for comparison (Figure 5). The hydrogen and oxygen stable isotopes of all water samples fall near GMWL and LMWL [29], suggesting that the recharge source is meteoric water. The δ^2H and $\delta^{18}O$ values of the hot springs in the WWFZ are significantly smaller than those of other waterbodies within the Gonghe Basin, suggesting that the hot water in the study area is derived from meteoric water at higher elevations or from meteoritic water in colder climate. Combined with the topography and geomorphology of the area, the WWFZ is located in the Ngola Shan Mountains with an average elevation of more than 4500 m. According to the elevation effect, the δ^2H and $\delta^{18}O$ values of the meteoric water gradually decrease with the increase of elevation, which makes the δ^2H and $\delta^{18}O$ values of the hot water in the area significantly smaller than that of the other water bodies in the neighboring Gonghe Basin. Based on the stable isotope intervals of ice melt water and magma water in the area, the possible range of magma water genesis was mapped, and no hot water in the area was found to have been influenced by magma water. The weak oxygen drifts in H01 and H02 indicate that water-rock interactions occurred at depth in the hot water, which is consistent with the results of the Gibbs diagram.

Preprints.org (www.preprints.org) | NOT PEER-REVIEWED | Posted: 11 April 2024 doi:10.20944/preprints202404.0757.v1

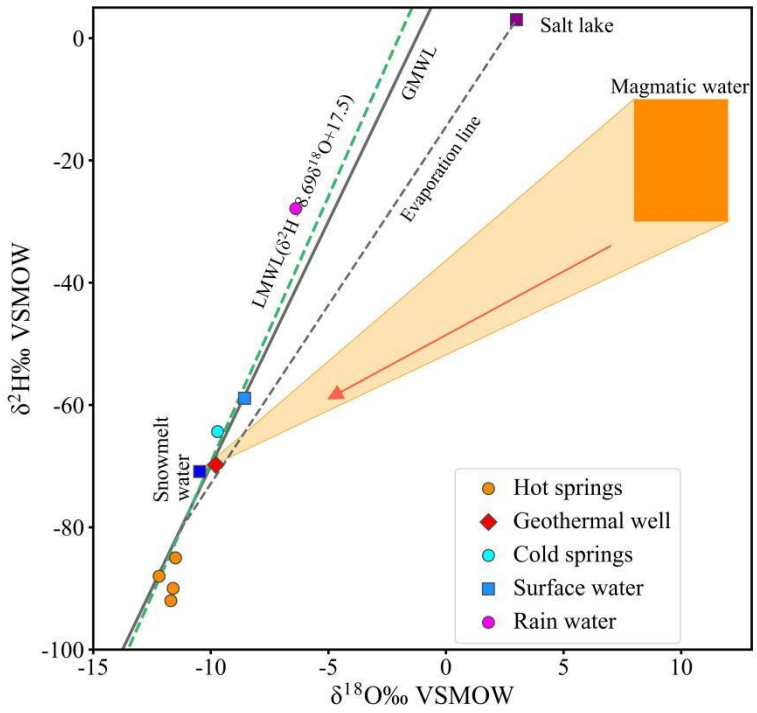

Figure 5. Stable isotope composition of different hot springs in WWFZ.

The recharge elevation of the hot spring water can be determined based on the elevation effect of meteoric water isotopes and is calculated as follows:

$$H = \frac{\delta s - \delta p}{k} + h$$

where H is the altitude of groundwater recharge; δs: is the isotope value of hot springs at the sampling point; δp: is the isotope value of meteoric water; k: is the value of isotope height gradient; h: is the height of the sampling point. The average value of the oxygen isotope of local rainwater was taken -7.97‰, and the value of the isotope height gradient was 3‰, and the calculation results are shown in Table 1. The altitude of the hot spring recharge area in the study area is between 5155-5525m, indicating that the recharge areas of the hot springs are all located in the central main ridge of Ngola Shan Mountains where they are located.

3.3. Chemical Characterization of Hot Spring Gases

3.3.1. Hot Spring Gas Composition

The gases in the hydrothermally active region of the Tibetan Plateau can be broadly divided into two categories: CO_2-dominated geothermal gases, known as CO_2-type gases, and N_2-type gases, which are mainly composed of N_2. The former has two types of genesis, magmatic hot water, and deep cycle, and the latter are all deep cycle genesis [30]. The gas concentration data of different hot water in the study area (Figure 6) shows that all the hot water has N_2 as the main component. The average value of N_2 concentration is greater than 80%, which is N_2 type gas, i.e., the hydrothermal activity in the study area is of deep cycle genesis. Among other conventional gases, H_2, H_2S, and SO_2 were not detected due to their low concentrations; the higher O_2 concentrations, especially in the hot spring water samples with higher temperatures, may be caused by the dissolution of atmospheric oxygen components in hot water during the ascent process. However, the contamination of the samples due to unregulated operation during sampling cannot be excluded. The atmospheric components were not corrected for in the present study with the aim of reflecting the real state of the hydrothermal activity area. Except for sample H06, which contains relatively high CO_2 concentration (7.83%), most of the samples contain low CO_2 concentration, with an average of only 0.7%.

 doi:10.20944/preprints202404.0757.v1

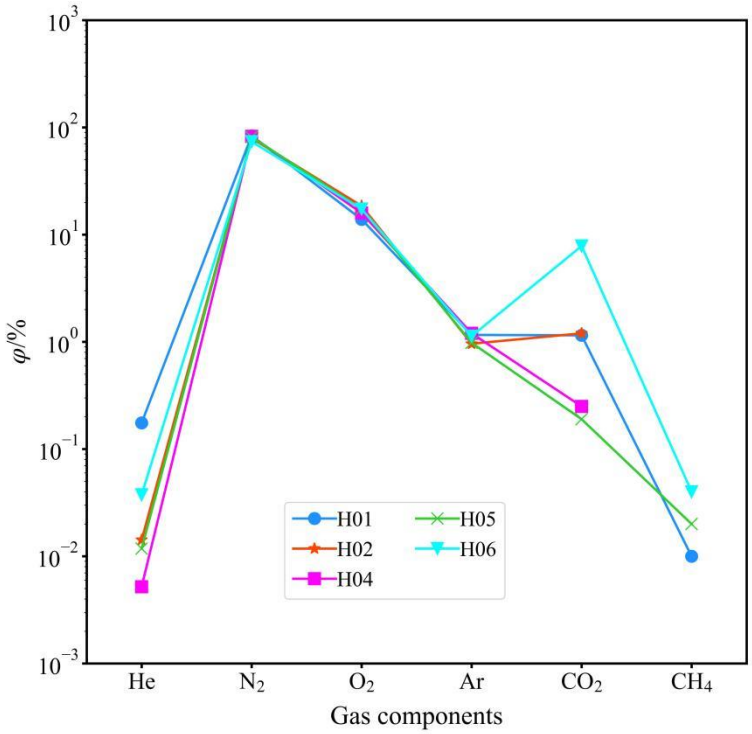

Figure 6. The chemical composition schoeller diagram of hot spring gases in WWFZ.

Nitrogen (N_2) is the constant gas component in low and medium-temperature geothermal systems. Nitrogen is weakly geochemically active and has a chemical stability similar to noble gases. N_2 in geothermal gases, along with Ar, is thought to originate from air dissolved prior to the recharge of geothermal water by meteoric water, after which the oxidizing gas components (e.g., oxygen) are depleted after long runoff in a reducing environment, resulting in the accumulation of rare gas components such as nitrogen and argon as the dominant component. He-Ar-N_2 diagrams Giggenbach and Glover (1992) show (Figure 7) that the N_2/Ar values of all samples fall within the interval between the meteoric water value (38) and the atmospheric value (84) and are closer to the atmospheric value (84), indicating that the N_2 component in the hot springs is dominated by atmospheric genesis [31]. The He component of the hot spring gases in the study area is mainly a product of the crust's radioactive decay of uranium and thorium. However, it cannot be excluded that individual samples (H01) are close to the vicinity of the He end (which usually represents mantle genesis), suggesting that the samples may have a tiny amount of mantle component added. Natural seismic profiles along the Gonghe Basin-Yushu highway show that the high-velocity and low-velocity bodies in the crust of Gonghe Basin are stacked vertically in the Wenquan Township, and the Chabcha area and the LVB are buried at a depth of 15-43 km in the Wenquan Township with the S-wave velocity of fewer than 3.4 km/s [32]. In recent years, in response to the exploration of the deep Hot Dry Rock in the Gonghe Basin, many scholars have studied the seismicity of the crust in this area, and most of them recognize it as a young (Quaternary) mantle-derived melt intruding into the crust [33–37]. Thus, degassing of the melt provides the possibility of the presence of the mantle component He in the surface hot springs.

Preprints.org (www.preprints.org) | NOT PEER-REVIEWED | Posted: 11 April 2024 doi:10.20944/preprints202404.0757.v1

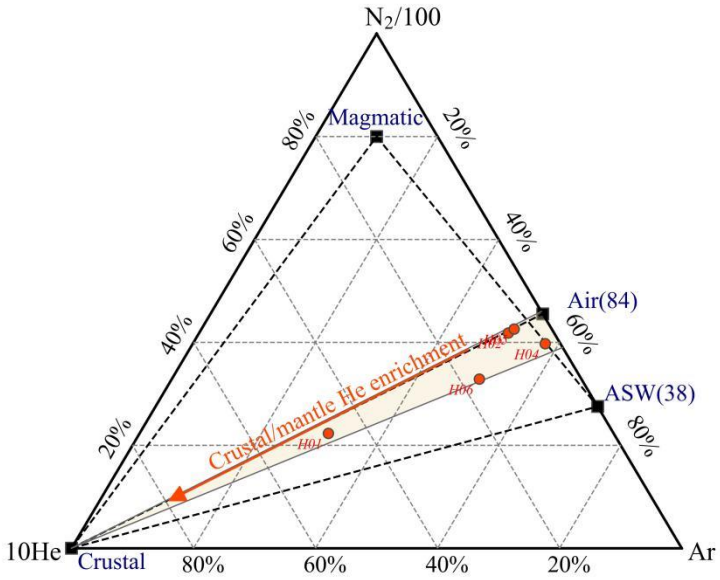

Figure 7. Relative He, Ar and N_2 contents of hot spring gases samples in WWFZ (Modified from [31]).

3.3.2. Isotopic Characterization of Hot Spring Gases

Helium (He) has two natural isotopes, ^{3}He and ^{4}He, and the vast majority of the release from mantle degassing is geogenic ^{3}He, which is accompanied by mantle heat transfer to shallow fluids during upward transport along tectonic channels. In contrast, the α-decay generation of ^{4}He from the natural radiative systems of ^{238}U, ^{235}U, and ^{232}Th in the crust is the primary source of helium within the crust [38]. Since the helium isotope ratios R (^{3}He/^{4}He) in the different source gases vary, the isotopic composition of atmospheric helium is usually used as a reference for comparison (Ra = 1.43 × 10^{-6}), e.g., the helium isotope ratio R in mid-oceanic ridge basalt (MORB), which represents the upper mantle, is about (8 ± 1) Ra, whereas the helium isotope ratios R in the crust are usually 0.005-0.02 Ra or so. Accordingly, the distribution of helium isotope ratios of hot spring gases can be used to analyze the regional geothermal background, fracture spreading pattern, fracture activity, and fluid circulation conditions.

Since atmospheric components are inevitably mixed into the samples due to operational errors during gas collection, Duchkov (2010) proposed correcting the R-value of geothermal gas samples with the ^{4}He/^{20}Ne ratio to remove the effect of atmospheric mixing during sampling[39]. The atmospheric ^{4}He/^{20}Ne ratio is about 0.318, i.e., if the ^{4}He/^{20}Ne of a sample is close to 0.318, it means that the helium in it is mainly of atmospheric origin, and the correction equation is as follows:

$$R_c = \left[R_m \times \left(^4He/^{20}Ne\right)_m - R_a \times \left(^4He/^{20}Ne\right)_a\right] / \left[\left(^4He/^{20}Ne\right)_m - \left(^4He/^{20}Ne\right)_a\right]$$

In the formula, the subscripts c, m, and a represent the atmospheric source's calibration value, test value, and characteristic value. Sano (1982) assumed that there are three sources of helium in natural gases: atmospheric, mantle, and crustal [40]. They proposed a formula for calculating the mixing ratio of the different sources in the gas samples by using the ratios of ^{3}He/^{4}He and ^{4}He/^{20}Ne, as well as a plot of the relationship of ^{3}He/^{4}He-^{4}He/^{20}Ne, which makes the method of determining the source of helium more simple and intuitive. The formulae for determining the source of helium are as follows:

$$\left(\frac{^3He}{^4He}\right)_{sample} = \left(\frac{^3He}{^4He}\right)_A \times f_A + \left(\frac{^3He}{^4He}\right)_M \times f_M + \left(\frac{^3He}{^4He}\right)_C \times f_C$$

$$\frac{1}{\left(^4He/^{20}Ne\right)_{sample}} = \frac{f_A}{\left(^4He/^{20}Ne\right)_A} + \frac{f_M}{\left(^4He/^{20}Ne\right)_M} + \frac{f_C}{\left(^4He/^{20}Ne\right)_C}$$

$$f_A + f_M + f_C = 1$$

 doi:10.20944/preprints202404.0757.v1

The subscripts A, M, and C represent atmospheric, mantle, and crustal sources, respectively, and f_A, f_M, and f_C represent the proportions of the three sources in the gas samples, of which $(^3He/^4He)_A=1.4\times10^{-6}$, $(^3He/^4He)_M=1.1\times10^{-5}$, $(^3He/^4He)_C=1.5\times10^{-8}$, $(^4He/^{20}Ne)_A=0.318$, $(^4He/^{20}Ne)_M=1000$, $(^4He/^{20}Ne)_C=0.1000$. The calculation results are shown in Table 3. He contents in the H01 and H05 gas samples mainly originates from the α-decay of the natural radiative systems of ^{238}U, ^{235}U, and ^{232}Th in the crust, and the average proportion reaches more than 97%. Plotting the $^3He/^4He$-$^4He/^{20}Ne$ relationship of the geothermal gases in the study area is shown in Figure 8, and the He isotope R/Ra values (ratio relative to the atmosphere) of the hot-water gases in these two locations fall into the crustal helium domain (<0.05), indicating that they are predominantly crustal in origin.

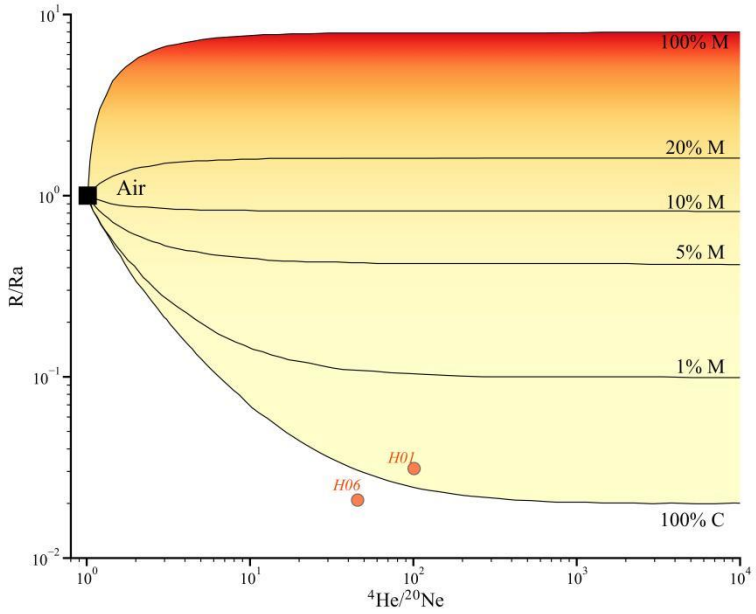

Figure 8. $^3He/^4He$-$^4He/^{20}Ne$ relations of hot spring gases in WWFZ.

3.4. Geothermal Reservoir Temperatures and Circulation Depths

3.4.1. Water-Rock Equilibrium Analysis

The Na-K-Mg triangulation diagram, proposed by Giggenbach (1988), is divided into three regions: fully equilibrated, partially equilibrated, and immature water, and is often used to evaluate water-rock equilibrium and to distinguish between different types of water samples[41]. The advantage of this method is that the equilibrium state of a large number of water samples can be determined simultaneously on the same map, and mixed and equilibrium waters can be well separated. The Na, K, and Mg contents of different hot springs in the study area were plotted on the Na-K-Mg equilibrium triangulation diagram (Figure 9), in which four hot springs are located in the immature water region at the apex of the lower-right corner, which indicates that they are still in the primary stage of water-rock interaction. The two hot springs, H03 and H05, are located in the partially equilibrated or mixed water region, reflecting that the ionic equilibrium between water and rock has yet to be reached. Dissolution is still in progress, or the hot water was mixed with the shallow cold water in the rising process. In addition, from the Na-K-Mg equilibrium triangulation diagram, it can be seen that the geothermal reservoir temperatures of all hot spring sites fall between 120°C and 270°C, with H06 having the highest potential geothermal reservoir temperature, which is consistent with the highest temperature of its spring water.

 doi:10.20944/preprints202404.0757.v1

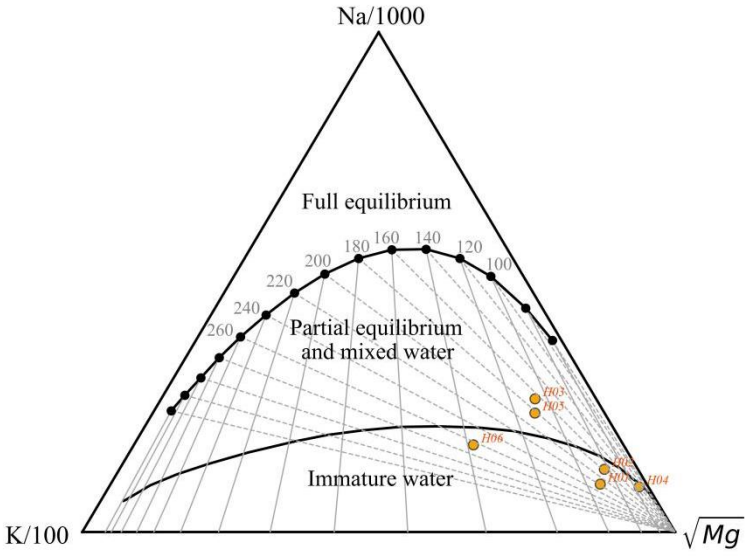

Figure 9. Na-K-Mg diagrams for various hot springs in WWFZ.

3.4.2. Estimation of Geothermal Reservoir Temperatures by Multi-Mineral Saturation Indices

Reed and Spycher (1983) proposed a multi-mineral equilibrium graphical method to determine the overall chemical equilibrium state between hydrothermal fluids and minerals in geothermal systems [42]. The principle is that the dissolved state of many minerals in the water is a function of temperature. Suppose a group of minerals at a particular temperature simultaneously is close to equilibrium. In that case, it can be judged that the hot water and the group of minerals reach equilibrium, and the equilibrium temperature is the temperature of the deep geothermal reservoir.

The degree of saturation of each mineral can be determined from the saturation index SI of the minerals in the geothermal water, with SI > 0 indicating oversaturation, SI = 0 indicating saturation, and SI < 0 indicating unsaturation:

$$SI = \log\left({}^{Q}/_{K}\right)$$

where, K - solubility of minerals in hot water, mol/L; Q - ionic activity product of minerals actually dissolved in hot water, mol/L.

Aluminum-bearing silicate minerals could not be produced because the aluminum concentration in the hot water in the study area was not detected below the detection limit. One or two Al-containing silicate minerals have reached equilibrium in most geothermal systems. Accordingly, Pang and Reed (1998) proposed using Al fixation to restore the equilibrium of Al-containing silicate minerals in geothermal systems [43]. Under multi-component, non-homogeneous chemical equilibrium conditions in geothermal systems, the equilibrium of aluminum-silicate minerals is interdependent because the minerals all contain specific chemical components. When the Al concentration is unknown, it can be estimated at different temperatures by assuming that the activity of Al is fixed by some aluminum-bearing mineral such as microplagioclase feldspar. A value for the Al concentration is obtained and then used to calculate Q/K values for other aluminosilicate minerals. This method of estimating Al concentration values is valid for a given geothermal water because most geothermal waters are in equilibrium with at least two aluminosilicate minerals.

We analyzed the equilibrium state of the hot water in the study area by immobilizing Al with microplagioclase feldspar. Based on the hydrochemical data of hot water in the study area, we calculated each mineral's saturation index SI value at different temperatures using the PHREEQCI program. We plotted the SI - T curve with temperature as the horizontal coordinate and log (Q/K) value as the vertical coordinate. Based on the rock mineral survey data in the study area, we selected 11 common minerals: quartz (Quartz), chalcedony (Chalcedony), potassium feldspar (K-feldspar), calcite (Calcite), fluorite (Fluorite), aragonite (Aragonnite), gypsum (Gypsum) and magnesite (

 doi:10.20944/preprints202404.0757.v1

Magnesite), and their SI-T curves (Figure 10) (H02 and H03 are located in the same geothermal field, and only the higher temperature H02 hot spring was calculated). Among them, the curves of H01, H02, H05, and H06 converged better, and their geothermal reservoir temperatures were 135℃, 139℃, 152℃ and 159℃, respectively, and the curve of H04 converged generally, and its geothermal reservoir temperature was about 80℃. H06 has the highest geothermal reservoir temperature among all hot springs, which is consistent with the highest temperature of its spring water.

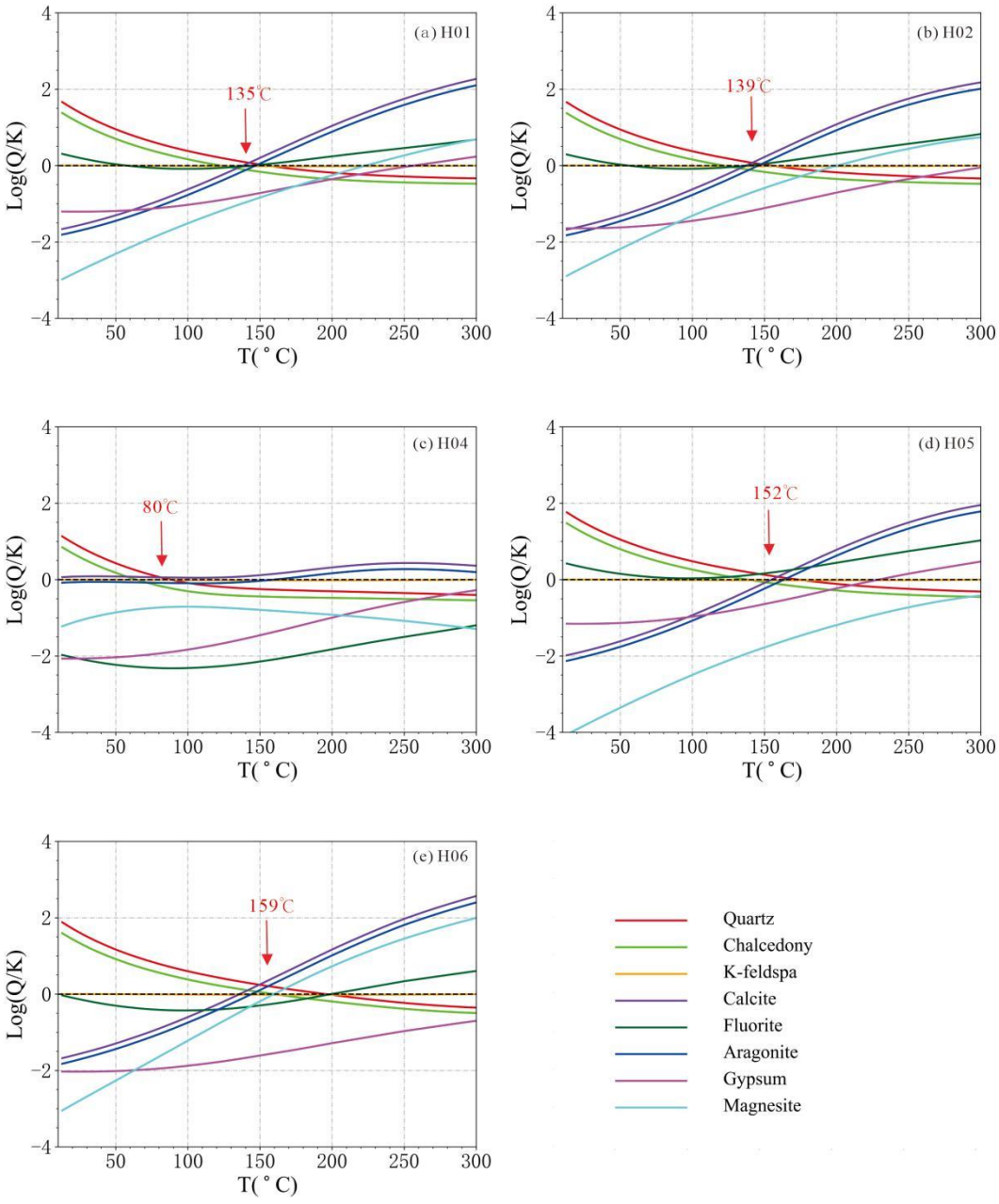

Figure 10. Mineral saturation diagram for the typical hot spring in WWFZ.

3.4.3. Geothermal Reservoir Temperature Estimation by Geothermometers

Geothermometers indirectly estimate geothermal reservoir temperatures based on the balance of minerals in the water. Geochemical geothermometers commonly used are cation geothermometers and silica geothermometers. However, the results of the estimation of reservoir temperature are often varied because the loss of volatile components of the geothermal system may affect the temperature estimation. Uncertainty in geothermal reservoir temperature estimation also increases due to the

 doi:10.20944/preprints202404.0757.v1

mixing of shallow groundwater that disturbs the original ionic equilibrium conditions [44]. According to the previous analysis, the hot spring waters in the study area are all immature or partially equilibrated (mixed), which do not meet the conditions for the use of cationic geothermometers, so we adopt the silica geothermometer for the estimation of the geothermal reservoir temperatures. The silica geothermometer is one of the most widely used methods for estimating geothermal reservoir temperatures. It is based on the fact that the silicon concentration in an aqueous solution is determined by the solubility of silicon at the temperature of the water-rock interaction. The total concentration of silicon is a function of temperature. When there is no vapor loss from hot water during its ascent to the surface or when only conduction cooling is present, the quartz silica geothermometer uses the no vapor loss expression. When hot water has a maximum steam loss at a given temperature during ascent to the surface or when adiabatic cooling is predominant, the maximum steam loss geothermometer expression is used. Calculations are shown in Table 4.

Table 4. Geothermal reservoir temperature estimated by different methods and circulation depth of hot springs.

ID	T（℃）	SiO_2 (maximum steam loss)	SiO_2 (no vapor loss)	Chalcedony	Silicon Enthalpy Diagram	multi-mineral saturation indices	Cold water mixing ratio/%	circulation depth/m
H01	64	121.2	123.6	95.5	193	135	71.0	2732-2985
H02	78	120.6	122.8	94.7	166	139	56.9	2714-3074
H04	44	96.8	95.1	64.7	168	80	79.0	1763-2098
H05	67	136.6	141.8	115.6	230	152	74.5	3136-3363
H06	85	139.0	144.6	118.7	205	159	62.4	3198-3518

3.4.4. Silicon Enthalpy Mixing Model for Estimating Cold Water Mixing Ratio

The Silicon Enthalpy Mixing Model (SEMM) estimates the mixing proportion of shallow cold water during hot spring ascent. This method obtains the mixing proportion of cold water and estimates the hot spring's geothermal reservoir temperature. However, according to Dong (2000), the result of the SEMM is too high, which may be due to the loss of steam from the expansion of the underground hot water before mixing with the cold water, and thus the SiO_2 content of the spring water is measured too high [45]. The overall geothermal reservoir temperatures calculated using the SEMM are relatively high (Table 4) and are for reference only. The results show a significant amount of cold water mixing in the springs throughout the study area, with the percentage of cold-water mixing ranging from 56.9-79.0%.

3.4.5. Hot Water Circulation Depth Estimates

The geothermal reservoir temperatures estimated by the water-rock equilibrium analysis of the hot springs in the study area as well as by the silica geothermometer, the multimineral equilibrium analysis, and the SEMM (Figure 11), the calculated results of the SEMM (blue line) are high. The results of the chalcedony geothermometer (green line) are low. In contrast, the quartz (no vapor loss) geothermometer results are the closest to the results of the multimineral equilibrium analysis. Therefore, we choose the interval (range bar) of the results of these two methods as the geothermal reservoir temperature interval of the hot springs in the study area (Figure 11).

 doi:10.20944/preprints202404.0757.v1

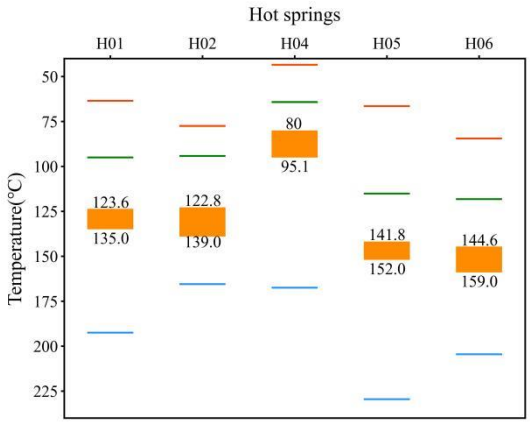

Figure 11. Geothermal reservoir temperatures of different hot springs in the study area obtained by different methods. The orange bar graph shows the range of geothermal reservoir temperatures determined by the quartz geothermometer (without vapor loss) and the multiple mineral saturation index method; the blue line indicates the geothermal reservoir temperature obtained from the silica-enthalpy mixing model; the green lines indicate the geothermal reservoir temperature obtained from the chalcedony geothermometer and the red line shows the temperature of the hot springs at the surface.

Geothermal water is usually warmed by heating from a deep heat source during deep circulation. The following formula roughly estimates the depth of hot spring circulation:

$$H = \frac{t - t_0}{k} + H_0$$

where t is the geothermal reservoir temperature, t_0 is the local average annual air temperature, k is the geothermal gradient, and H_0 is the depth of the normal temperature zone.

According to the monitoring data, the average annual temperature of the Xinghai, Wulan, and Dulan area is 2.7℃, and the depth of the normal temperature zone is about 45m. The geothermal temperature gradient is about 4.5℃/100m, and the range of circulating depths of different hot water springs obtained from the calculations is shown in Table 4. Among them, the circulating depth of H06 is the deepest, about 3,198-3,518m, and the hot water circulating in H04 is the shallowest, which is only about 1,763-2,098m.

4. Discussion

Fractures are the most prevalent heat-controlling structures on Earth. According to the depth of its cut through each tectonic layer can be divided into the lithospheric fracture, which cuts through the entire lithosphere to the top of the upper mantle; the crustal fracture, which cuts through the entire crust to the Moho discontinuity; the basement fracture, cut through the upper crust of the entire "granitic layer," to the Conrad discontinuity; cover fracture, cut through the sedimentary cover, to the top of the metamorphic basement; interlayer Slip fractures, varying in depth, the deeper ones being associated with giant uplift and depression tectonic movements, the shallower ones with folds. Certain fractures, or some parts of them, are often favorable channels for water (hot or cold) and magmatic activities, which may affect the geothermal conditions in a particular range and to a certain extent, thus forming geothermal anomaly zones. The WWFZ is a crustal fracture that cuts through the entire crust and contacts the upper mantle, which is favorable for mantle heat flow to be transported upward along the fracture, forming a regional heat-controlling fracture. At the same time, the fracture is cut by a small number of small-scale near-north-south and near-east-west fractures, and these fracture systems with different depths and crisscrosses provide favorable channels for deep hot water convection circulation in the region. By comparing and analyzing the fluid geochemical characteristics, geothermal reservoir depth, recharge height, and heat source mechanism of different hot springs within the WWFZ, a model of the water-heat cycle in the WWFZ fracture zone has been established (Figure 12).

 doi:10.20944/preprints202404.0757.v1

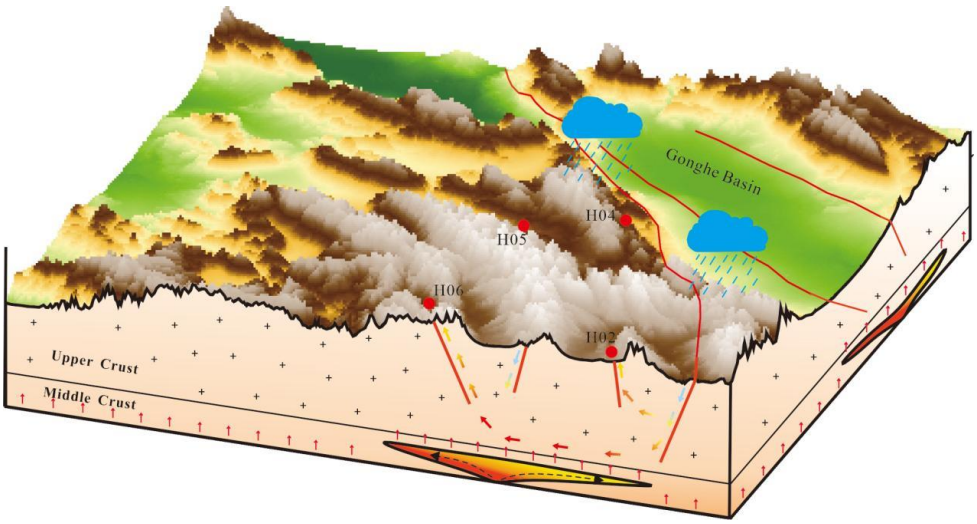

Figure 12. Hot spring formation pattern in the WWFZ.

Source: Includes water and heat sources. The δ^2H and $\delta^{18}O$ values of all hot springs in the WWFZ-Hot Springs fracture zone are significantly lower than those of other water bodies in the Gonghe Basin, suggesting that the hot spring water in the study area is recharged from meteoric water at higher elevations or from meteorite water in colder climates. According to the hydrogen and oxygen isotopes of the hot water, the recharge elevation was estimated to be between 5155 and 5525 m, which means that all the hot spring water came from the snow and ice meltwater of Ngola Shan Mountains at an elevation of more than 5100 m above sea level. The gas test results show that all the hot springs in the area are N_2-type gases, i.e., the hot water is caused by deep-cycle heating. The He isotopes of the gases fall into the helium domain of the crust, i.e., the gases are mainly generated by α-decay of the natural radioactive systems of ^{238}U, ^{235}U, and ^{232}Th in the crust, with no additional heat contribution from the mantle source. Low-velocity bodies of unknown nature in the lower and middle crust of the region may have provided an additional source of heat to the high-temperature thermal background of the study area, where hot springs were formed by deep circulation heating of snow and ice meltwater.

Channel: The northwesterly Wahongshan-Wenquan fracture and the transverse near-north-south or near-east-west fracture form a fracture system that provides a favorable channel for the deep hot water convection circulation in the study area. According to the fluid geochemical characteristics of different hot springs in the area, the hot springs can be categorized into two runoff channels: long and short. Hot springs near the primary fracture of the WWFZ have relatively short runoff pathways, better deep hydrodynamic conditions, relatively open underground environments, and lower TDS of hot water. Away from the primary fracture, the Na^+ and Cl^- ions content in the hot springs increased significantly, and the groundwater circulation rate slowed down, showing the characteristics of deep circulation and long runoff type.

Reservoir: The study area is a convective geothermal reservoir system, and the fracture system formed by the north-west-trending WWFZ and a small number of fractures that transect the near-north-south or near-east-west direction constitutes the primary geothermal reservoir system. Except for H04, which has a low geothermal reservoir temperature (about 80-95.1°C) due to its shallow hot-water runoff depth of about 1763-2098m, the rest of the hot springs have a geothermal reservoir temperature higher than 120 degrees, and the highest one is located in H06, with a high geothermal reservoir temperature of 144.9-159.0°C, and accordingly, its hot-water runoff is also the deepest (3198-3518m).

Cover: For convective geothermal systems, the role of the cover is generally not noticeable. The poor hydrodynamic conditions (large $\gamma Cl^-/\gamma Ca^{2+}$ values) of the H02 and H03 hot springs near the primary fracture may be related to the thicker quaternary cover of the intermountain valley in which they are located.

 doi:10.20944/preprints202404.0757.v1

5. Conclusions

The Wanghongshan-Wenquan Fracture Zone (WWFZ) is located on the northeastern margin of the Tibetan Plateau, a crustal fracture that constitutes a regional heat-control tectonics. The fracture system formed by a few near-north-south and near-east-west oriented fractures that cut across the WWFZ provides a favorable channel for deep water-heat convection circulation. The intersection of these fractures is where the region's hot springs are centrally exposed. The degree of research on the geothermal heat of the WWFZ still needs to be higher, and the information needs to be more extensive. In this paper, we analyze the hydrothermal processes of five hydrothermal activity zones occurring in the fracture zone, mainly in terms of differences in fluid chemistry and isotopic compositions of hot water, aiming to help future geothermal development in the zone. The hydrochemical characteristics of the different hot springs in the zone indicate that the ice and snow melt water of Ngola Shan Mountains, with an average elevation of over 4500m, is the source of recharge, and the ice and snow melt water infiltrates along the fracture and is heated by the deep cycle to form deep geothermal reservoirs. There is no detectable contribution of mantle source heat in the hot spring gas, and its heat source is mainly natural conduction or convective warming, but the "low-velocity layer" of the middle and lower crust in the area may be the primary heat source of the high geothermal background in the area. The water chemistry of the hot springs in the area shows a certain regularity. Away from the primary fracture, the main ionic components, TDS, and water temperature tend to increase, reflecting the controlling effect of the WWFZ on the water and heat in the area. Future geothermal work in this area should focus on the hydrothermal control properties of different levels, the nature of fractures in the area, and the thermal contribution of low-velocity bodies in the middle and lower crust.

Author Contributions: Conceptualization, W.L. and T.L.; methodology, W.L.; software, T.L.; validation, R.L., W.X. and W.L.; formal analysis, T.L.; investigation, L.L.; resources, J.Z.; data curation, T.L.; writing—original draft preparation, T.L.; writing—review and editing, W.L.; visualization, L.L.; supervision, J.Z.; project administration, R.L.; funding acquisition, W.L. All authors have read and agreed to the published version of the manuscript.

Funding: This research was funded by the National Key Research and Development Program of China (Grant No. 2021YFB1507401), Qinghai Province Clean Energy Minerals Special Project (No. 2022013004qj004) and Geological Survey Project of China Geological Survey (No. DD20221676, NO.DD20230019).

Data Availability Statement: Data are contained within the article.

Conflicts of Interest: The authors declare no conflicts of interest.

References

1. Liao, Z., 2018. Thermal Springs and Geothermal Energy in the Qinghai-Tibetan Plateau and the Surroundings. Springer Singapore, https://doi.org/10.1007/978-981-10-3485-5.
2. Wang, Guiling, Lin, Wenjing. 2020. Main hydro- geothermal systems and their genetic models in China. Acta Geologica Sinica 94(7), 1923-1937. https://doi.org/10.19762/j.cnki.dizhixuebao.2020224.
3. Wang, Y., Li, L., Wen, H., Hao, Y., 2021a. Geochemical evidence for the nonexistence of supercritical geothermal fluids at the Yangbajing geothermal field, southern Tibet, Journal of Hydrology 604, 127243. https://doi.org/10.1016/j.jhydrol.2021.127243.
4. Yu, X., Wei, Z., Wang, G., Ma, X., Zhang, T., Yang, H., Li, L., Zhou, S., Wang, X., 2022. Hot spring gas geochemical characteristics and geological implications of the northern Yadong-Gulu Rift in the Tibetan Plateau. Front. Earth Sci. 10, 863559. https://doi.org/10.3389/feart.2022.863559.
5. Zhao, D., Zhou, X., Zhang, Y., He, M., Tian, J., Shen, J., Li, Y., Qiu, G., Du, F., Zhang, X., Yang, Y., Zeng, J., Rui, X., Liao, F., Guan, Z., 2023. Hydrogeochemical Study of Hot Springs along the Tingri—Nyima Rift: Relationship between Fluids and Earthquakes. Water 15, 1634. https://doi.org/10.3390/w15081634.
6. Ye, T., Huang, Q., Chen, X., Zhang, H., Chen, Y. J., Zhao, L., Zhang, Y., 2018. Magma chamber and crustal channel flow structures in the Tengchong volcano area from 3-D MT inversion at the intracontinental block boundary southeast of the Tibetan Plateau. Journal of Geophysical Research: Solid Earth 123, 11,112–11,126. https://doi.org/10.1029/2018JB015936.

7. Zhang, M., Liu, W., Guan, L., Takahata, N., Sano, Y., Li, Y., Zhou, X., Chen, Z., Cao, C., Zhang, L., Lang, Y., Liu, C., Xu, S., 2022a. First estimates of hydrothermal helium fluxes in continental collision settings: Insights from the Southeast Tibetan Plateau margin. Geophysical Research Letters 49, e2022GL098228. https://doi.org/10.1029/2022GL098228.
8. Zhou, X., Liu, L., Chen, Z., Cui, Y., Du, J., 2017. Gas geochemistry of the hot spring in the Litang fault zone, Southeast Tibetan Plateau. Applied Geochemistry 79, 17-26. https://doi.org/10.1016/j.apgeochem.2017.01.022.
9. Zhao, J., Wang, G., Zhang, C., Xing, L., Li, M., Zhang, W., 2021. Genesis of geothermal fluid in typical geothermal fields in western Sichuan, China. Acta Geologica Sinica-English edition 95(3), 873-882. https://doi.org/10.1111/1755-6724.14715.
10. Tian, T., Pang, Z., Liao, D., Zhou, X., 2021. Fluid geochemistry and its implications on the role of deep faults in the genesis of high temperature systems in the eastern edge of the Qinghai Tibet Plateau. Applied Geochemistry 131, 105036. https://doi.org/10.1016/j.apgeochem.2021.105036.
11. Sun, M.; Zhang, X.; Yuan, X.; Yu, Z.; Xiao, Y.; Wang, Y.; Zhang, Y. 2022. Hydrochemical Characteristics and Genetic Mechanism of Geothermal Springs in the Aba Area, Western Sichuan Province, China. Sustainability 14, 12824. https://doi.org/10.3390/su141912824.
12. Wang, C., Zheng, M., Zhang, X., Wu, Q., Liu, X., Ren, J., Chen, S., 2021b. Geothermal-type lithium resources in southern Xizang, China. Acta Geologica Sinica-English edition 95(3), 860-872. https://doi.org/10.1111/1755-6724.14675.
13. Liu, J., Zhou, X., Li, Y., He, M., Li, J., Dong, J., Tian, J., Yan, Y., Ouyang, S., Liu, F., 2023a. Relationship between hydrogeochemical characteristics of hot springs and seismic activity in the Jinshajiang fault zone, Southeast Tibetan Plateau. Front. Earth Sci. 10, 1015134. https://doi.org/10.3389/feart.2022.1015134.
14. Liu, F., Zhang, W., Wang, G., Wei, S., Yue, C., Jiang, G., Liao, Y., 2023b. Geothermal anomalies in the Xianshuihe area: Implications for tunnel construction along the Sichuan-Tibet Railway, China. Journal of Groundwater Science and Engineering 11(3), 237-248. https://doi.org/10.26599/JGSE.2023.9280020.
15. Lin, W., Wang, G., Shao, J., Gan, H., Tan, X.. 2021a. Distribution and exploration of hot dry rock resources in China: progress and inspiration. Acta Geologica Sinica 95(5), 1366-1381. https://doi.org/10.19762/j.cnki.dizhixuebao.2021213.
16. Zhang, C., Jiang, G., Shi, Y., Wang, Z., Wang, Y., Li, S., Jia, X., Hu, S., 2018. Terrestrial heat flow and crustal thermal structure of the Gonghe-Guide area, northeastern Qinghai-Tibetan plateau. Geothermics 72, 182-192. https://doi.org/10.1016/j.geothermics.2017.11.011.
17. Zhang, S., Zhang, L., Tian, C., Cai, J, Tang, B., 2019. Occurrence geological characteristitics and development potential of hot dry rocks in Qinghai Gonghe basin. Journal of Geomechanics 25, 501-508. https://doi.org/10.12090/j.issn.1006-6616.2019.25.04.048.
18. Long, D., Zhou, X., Yang, K., Gu, P., Gao, Y., Wang, S., Chen, G., 2021. Research on relationship between the deep structure and geothermal resource distribution in the Northeastern Tibetan Plateau. Geology in China 48(3), 721-731. https://doi.org/10.12029/gc20210304.
19. Lin, W., Wang, G., Zhang, S., Zhao, Z., Xing, L., Gan, H., Tan, X., 2021b. Heat aggregation mechanisms of Hot Dry Rocks resources in the Gonghe Basin, northeastern Tibetan Plateau. Acta Geologica Sinica - English Edition 95(6), 1793-1804. https://doi.org/10.1111/1755-6724.14873.
20. Song, G., Song, X., Li, G., Xu, R., Cao, W., Zhao, C., 2021. Multi-objective optimization of geothermal extraction from the Enhanced Geothermal System in Qiabuqia geothermal field, Gonghe Basin. Acta Geologica Sinica-English edition 95(6), 1844-1856. https://doi.org/10.1111/1755-6724.14875.
21. Zhang, E., Wen, D., Wang, G., Yan, W., Wang, W., Ye, C., Li, X., Wang, H., Tan, X., Weng, W., Li, K., Zhang, C., Liang, M., Luo, H., Hu, H., Zhang, W., Zhang, S., Jin, X., Wu, H., Zhang, L., Feng, Q., Xie,J., Wang, D., He, Y., Wang, Y., Chen, Z., Cheng, Z., Luo, W., Yang, Y., Zhang, H., Zha, E., Gong, Y., Zheng, Y., Jiang, C., Zhang, S., Niu, X., Zhang, H., Hu, L., Zhu, G., Xu, W., Niu, Z., Yang, L., 2022b. The first power generation test of hot dry rock resources exploration and production demonstration project in the Gonghe Basin, Qinghai Province, China. China Geology 5, 372-382. https://doi.org/10.31035/cg2022038.
22. Lin, W., Wang, G., Gan, H., Zhang, S., Zhao, Z., Yue, G., Long, X., 2023. Heat source model for Enhanced Geothermal Systems (EGS) under different geological conditions in China, Gondwana Research, 122, 243-259. https://doi.org/10.1016/j.gr.2022.08.007.
23. Zhang, X., Guo, Q., Liu, M., Luo, J., Yin, Z., Zhang, C., Zhu, M., Guo., W., Li, J., Zhou, C., 2016. Hydrogeochemical processes occurring in the hydrothermal systems of the Gonghe–Guide basin,

northwestern China: critical insights from a principal components analysis (PCA). Environ Earth Sci 75, 1187. https://doi.org/10.1007/s12665-016-5991-9.

24. Ma, Y., Tang, B., Su, S., Zhang, S., Li, C., 2020. Geochemical characteristics of geothermal fluids and water-rock interaction in geothermal reservoirs in and around the Gonghe Basin, Qinghai Province. Earth Science Frontiers 27(1), 123-133. https://doi.org/10.13745/j.esf.2020.1.14.
25. Wang, B.; Qin, X.; Ren, E.; Feng, N.; Yang, S.; Li, W.; Li, G.; Jiang, Z., 2023a. Geochemical characteristics and formation mechanisms of the geothermal waters from the Reshui area, Dulan of Qinghai, China. Water 15, 3084. https://doi.org/10.3390/w15173084.
26. Wang, G., Lin, W., Liu, F., Gan, H., Wang, S., Yue, G., Long, X., Liu, Y., 2023b. Theory and survey practice of deep heat accumulation in geothermal system and exploration practice. Acta Geologica Sinica 97, 639-660. https://doi.org/10.19762/j.cnki.dizhixuebao.2023016.
27. Yuan, D., Zhang, P., Liu, B., Gan, W., Mao, F., Wang, Z., Zheng, W., Guo, H., 2004. Geometrical imagery and tectonic transformation of Late Quaternary active tectonics in northeastern margin of Qinghai-Xizang Plateau. Acta Geologica Sinica 78(2), 270-278.
28. Mondal, N.C., Singh, V.P., Singh, V.S., Saxena, V.K., 2010. Determining the interaction between groundwater and saline water through groundwater major ions chemistry. Journal of Hydrology 388(1-2), 100-111. https://doi.org/10.1016/j.jhydrol.2010.04.032.
29. Wu, H., Li, X., Zhao, G., Li, G., Li, Z., Li, L., 2014. The variation characteristics of δ18O and δD in precipitation and river water, Qinghai Lake Basin. Journal of Natural Resources 29(9), 1552-1564. https://doi.org/10.11849/zrzyxb.2014.09.010.
30. Zhao, P., Xie, E., Dor, J., Jin, J., Hu, X., Du, S., Yao, Z., 2002. Geochemical charact eristics of geothermal gases and their geological implications in Tibet. Acta Petrologica Sinica 18(4), 539-550.
31. Giggenbach, W.F., Glover, R.B., 1992. Tectonic regime and major processes governing the chemistry of water and gas discharges from the rotorua geothermal field, New Zealand. Geothermics 21(1-2), 121-140. https://doi.org/10.1016/0375-6505(92)90073-I.
32. Jiang, M., Wang, Y., Qian, H., 2009. The broadband seismicexploration as well as the crust upper mantle structure inthe orogenic plateau, Qinghai-Tibet plateau and itsadjacent area. Geological Publishing House, Beijing.
33. Feng, Y., Zhang, X., Zhang, B., Liu, J., Wang, Y., Jia, D., Hao, L., Kong, Z., 2018. The geothermal formation mechanism in the Gonghe Basin: Discussion and analysis from the geological background. China Geology 1, 331-345. https://doi.org/10.31035/cg2018043.
34. Gao, J., Zhang, H., Zhang, S., Chen, X., Cheng, Z., Jia, X., Li, S., Fu, L., Gao, L., Xin, H., 2018. Three-dimensional magnetotelluric imaging of the geothermal system beneath the Gonghe Basin, Northeast Tibetan Plateau. Geothermics 76, 15-25. https://doi.org/10.1016/j.geothermics.2018.06.009.
35. Gao, J., Zhang, H., Zhang, H., Zhang, S., Cheng, Z., 2020. Three-dimensional magnetotelluric imaging of the SE Gonghe Basin: Implication for the orogenic uplift in the northeastern margin of the Tibetan plateau. Tectonophysics 789, 228525. https://doi.org/10.1016/j.tecto.2020.228525.
36. Zhang, C., Hu, S., Song, R., Zuo, Y., Jiang, G., Lei, Y., Zhang, S., Wang, Z., 2020. Genesis of the hot dry rock gethermal resoureces in the Gonghe basin: constraints from the radiogenic heat production rate of rocks. Chinese Journal of Geophysics 63(7), 2697-2709. https://doi.org/10.6038/cjg2020N0381.
37. Zhou, W., Li, Q., Zhang, D., Tang, H., 2023. Crustal structure and geothermal mechanism of the Gonghe-Guide Basin based on EIGEN-6C4 satellite gravity and aeromagnetic data. Pure Appl. Geophys. 180, 2735–2756. https://doi.org/10.1007/s00024-023-03290-2.
38. International Atomic Energy Agency(IAEA), 2002. Isotopic and Chemical Techniques in Geothermal Exploration, Development and Use: Sampling Methods, Data Handling, Interpretation - Edited by Stefán Arnórsson, Non-serial Publications , IAEA, Vienna.
39. Duchkov, A.D., Rychkova, K.M., Lebedev, V.I., Kamenskii, I.L., Sokolova, L.S., 2010. Estimation of heat flow in Tuva from data on helium isotopes in thermal mineral springs. Russian Geology and Geophysics 51(2), 209-219. https://doi.org/10.1016/j.rgg.2009.12.023.
40. Sano, Y., Tominaga, T., Nakamura, Y., Wakita, H., 1982. 3He/4He ratios of methane-rich natural gases in Japan, Geochemical Journal 16(5), 237-245. https://doi.org/10.2343/geochemj.16.237.
41. Giggenbach, W.F., 1988. Geothermal solute equilibria. Derivation of Na-K-Mg-Ca geoindicators. Geochimica Et Cosmochimica Acta 52, 2749-2765. https://doi.org/10.1016/0016-7037(88)90143-3.

 doi:10.20944/preprints202404.0757.v1

42. Reed, M., Spycher, N., 1983. Calculation of pH and mineral equilibria in hydrothermal waters with application to geothermometry and studies of boiling and dilution. Geochimica et Cosmochimica Acta 48, 1479-1492. https://doi.org/10.1016/0016-7037(84)90404-6.
43. Pang, Z., Reed, M., 1998. Theoretical chemical thermometry on geothermal waters: problems and methods. Geochimica et Cosmochimica Acta 62, 1083-1091. https://doi.org/10.1016/S0016-7037(98)00037-4.
44. Liu, Y., Liu, B., Lu, C., Zhu, X., Wang, G., 2017. Reconstruction of deep fluid chemical constituents for estimation of geothermal reservoir temperature using chemical geothermometers. Journal of Groundwater Science and Engineering 5(2), 173-181. https://doi.org/10.26599/JGSE.2017.9280017.
45. Dong, W., Liao, Z., Liu, S. 2000. Geothermal in Tibet. Beijing: Science Press, 1-300.